

Aerodynamic Blade Optimal Design Of Turbomachinery

Ryoichi S. AMANO¹ and Cheng XU²

¹ Department of Mechanical Engineering
University of Wisconsin

Milwaukee, WI, 53201, U.S.A.

Phone: 414-229-2345, FAX: 414-229-6958, E-mail: amano@uwm.edu

²Siemens Westinghouse

¹ABSTRACT

For years dimensional blading has been used in the process of turbomachine designs. To meet the need for efficient turbine blade designs, CFD predictions of a complex 3D flow field in turbine blade passages had been used. Because the numerous advantages of 3-D CFD have been reported in the open literature, many industries already use 3D blading in their turbomachines. In addition, blade lean and sweep have been implemented to increase the blade row efficiency. Experimental studies have shown the advantages of these features. However, most of the experimental results combined other features together, which is difficult to determine the effects of individual features. In this study, the numerical study was presented to study the sweep effects of a transonic compressor airfoil.

INTRODUCTION

Most gas turbine designs still use throughflow and meanline codes as primary design tools. The throughflow calculation is based on a quasi-three-dimensional method to predict the flow on a stream surface. For most design cases, a throughflow code gives good solutions when compared with experimental data. When the pressure ratios of the turbines and compressors increase, the blade-to-blade Mach number becomes supersonic. For improving the blade designs, three-dimensional blades appear to reduce shock wave losses (Bliss, 1976). Moreover, for increasing turbine and compressor efficiency, bow, lean and sweep blades have demonstrated secondary flow and shock losses reduction. Because a throughflow analysis can not give a good estimation of three-dimensional blade flow structures, three-dimensional CFD codes (Xu and Amano, 2000a; Xu and Amano, 2000b; Xu and Amano, 2001a; Singh, et al., 1995) were developed to predict the flow structures of three-dimensional blades. Thus, in recent years three-dimensional codes have become one of the design tools in turbine design processes (Xu and Amano 2001b).

For most cases of a blade row in an annulus, the stream surface between two annular walls is twisted. These twists tend to induce either shed vortices or secondary flows arising from the inlet vortices. A stream surface twist can arise in an irrotational flow because of either spanwise velocity components or spanwise blade forces. Many efforts have been made to reduce the stream surface twist and the secondary flow losses, including developing alternative blades, such as sweep (Xu and Amano, 2000b), lean (Xu and Amano, 2001a), bow (Singh et al., 1995) and twist (Xu and Amano 2001b; Rabe et al., 1991) of the blades, or making a non-axisymmetric end-wall design. However, there is little

information in the open literature regarding the three-dimensional features because not many tests were performed before they are confidently adopted them in the manufacturing processes. Most of the studies have been still conducted at academic and scientific research organizations, which were based on particularly simple blade geometry and single stage or row flow conditions. For example, Singh et al (1995) reported that closing the blade throat near the end-walls could result in significant efficiency improvements because less fluid passed through the high loss regions. This closure tends to make the flow leaving the stator row less uniform with low axial velocities near the end-walls. However, the blade also integrates other changes, such as the end wall twist. Walker and Denton (1998) achieved an efficiency increase using almost the opposite type of blade twist near the end wall. They explained for this enhancement that opening of the blade throat at end-walls could twist the flow leaving the blade more uniform. However, they also made several simultaneous design changes on the original shape of the blade. It is necessary to investigate the effects of single blade feature change to guide the future blade design.

A sweep blade is widely used both in turbines and compressors (Denton and Xu, 1999). A sweep blade was first used (Bliss, 1976) to decrease the noise level induced by shock waves. However, the sweep design of the rotor did not increase the efficiency and reduce the noise level like a sweep wing. A more careful sweep design improved rotor efficiency; however, according to Rabe et al. (1991), the pressure ratio was lower than design intended. Recently, Hah, et al. (1999) studied both backward- and forward-swept leading edge compressor blades. Their study showed that an backwardsweep could suppress the intensity of the shock loss and a forward-swept rotor-blade could suppress the radial-wise secondary flow and tip entropy generation. The effects on efficiency were not great, but the backwardswept blade suffered a loss of stall margin because a shock appeared near the leading edge. Conversely, the forward sweep could increase the stall margin. The study by Xing, et al. (2001) showed that a stall margin of the back sweep is about the same as that of the unswept rotor blade. Clearly, the effects of sweep on transonic compressors are not fully understood. There are not many detailed descriptions of sweeps and whether other design parameters change or not when sweeps were implemented. Most studies (Hah et al., 1999; Wadia et al., 1997; Xing et al., 2001) did not report whether the flow boundary conditions were the same for all sweeps and unsweeps. Much research still need to be done to better understand sweep blades in the future. In addition, it is important to maintain all the other design parameters and flow boundary conditions. This paper attempts to numerically demonstrate sweep effects while maintain all the other design parameters and the flow conditions.

¹Copyright © 2003 by GTSJ

Manuscript Received on March 31, 2003

MATHEMATICAL MODEL

Numerical Method

Many three-dimensional, turbulent CFD codes have been developed based on the Reynolds averaged Navier-Stokes equations (Xu and Amano, 2000a&2000b). In these systems either the time-marching or the pressure based method is typically used in computations of the blade-to-blade passage flowfield. These traditional codes are limited in that each code can only predict either a compressible or incompressible flow well. Recently, Ho and Lakshminarayana (1996) have reported a CFD study in the secondary flow analysis where the calculation is based on a high-turning linear turbine cascade. More recently, the authors of these study (Xu and Amano, 2001a&2001b)] developed a time-marching scheme to predict two- and three-dimensional turbine and compressor flows and heat transfer analyses, a scheme which can compute both compressible and incompressible flows. The basic idea of the method is to effectively use the artificial viscosity components and modify the Navier-Stokes equations by incorporating the artificial viscosity components in the time-dependent terms. With these treatments, the method can avoid the eigenvalue stiffness problem for low Mach number flows by keeping the solutions within a reasonable accuracy range in addition it can subsequently demonstrate effective calculation capability for both low and high Mach number flows.

The viscous solver consists of three parts: mesh generation, N-S solver, and turbulence closure. The optimum grid type has been discussed for many years regarding which method should be used for turbine and compressor blade flow calculations (Xu and Amano, 2001b). The more orthogonal the grids, the smaller the numerical errors because truncation errors are reduced. However, no type of grid is ideal for blade-to-blade flow calculations. This study the H-type mesh is used as shown in Fig. 1. As far as the turbulence models are concerned, there remains controversy as to which models serve as the best turbulence and transition models in the computations. Even the number of mesh points employed necessary within the boundary layer for the same turbulence model still strongly depends on the case and the type of the N-S solver. This study employes the Baldwin-Lomax turbulence model for the flow analysis due to its favorable features for blade flow calculations (Xu and Amano, 2001b).

Numerical Model

In this study, four different compressor single rotor blade rows were calculated. All calculation cases involve same inlet and outlet conditions. Several types of boundary conditions have been used in the present study. Periodic boundaries were treated just as if they were interior points. The inlet total pressure profile flow angle and outlet static pressure were all taken from a multistage throughflow analysis (Xu and Amano, 2002). Other flow variables were extrapolated from interior points for inlet and outlet flow. The boundary conditions on the blade surfaces are those appropriate to the flow with no slip. The mesh size used in the calculations was $100 \times 35 \times 41$. After mesh independent studies, which showed that this mesh size is adequate. The calculated blade had an inner radius of 0.5m and an outer radius of 0.92mm with tip clearance of 1.0% of base section chord. The blade was designed in eleven sections, all the section shapes maintain same for all swept and based line cases. The calculation results showed that, for all the cases, the mass flow difference is less than 0.5%. Four different cases were reported here: baseline gravity center stackup blade, forward swept blade, backward swept and root partial swept blade.

The sweep was defined in two different ways (Hah, et al., 1999; Xing et al., 2001): one is using the leading edge sweep angle, and the other using the direct leading edge axial location. Using the axial location was convenient during the airfoil design process (Xu and Amano, 2002) because changes in the axial location impact the shifting of the section gravity center location, which will impact blade structure frequency and stresses. In most of the sweep airfoil studies, some sections of the airfoil chord lengths were changed

(Denton and Xu, 1999; Xing et al., 2001) and the locations of the airfoil base section also changed, which makes it difficult to see the sweep effects. In this study, the base section was fixed, more reasonable during new machine design and upgrade. The sweeps were also selected within the mechanically acceptable regions. The sweeps were defined as a nondimensional parameter: the ratio of leading edge axial distance change related to root section (DX) and axial chord (C). The axial changes from baseline location over the base section axial chord are shown in Fig. 2. Based on past experience [2-4], all calculations used the same convergent criteria during the calculation; i.e. RMS error should be smaller than 5.0×10^{-7} and the mass flow error smaller than 5.0×10^{-4} . The typical convergent history is shown in Fig. 3.

RESULTS AND DISCUSSION

The loss coefficient is defined as the total pressure drop over the outlet dynamic head. The mass average overall losses at exit plane are listed in Table 1. The calculations show that the baseline and backward sweep blades have relative larger losses than the forward and partial forward blades. However, the results of losses for sweeps do not depict large improvements, which is similar to some experiments (Bliss, 1976; Denton and Xu, 1999; Hah et al., 1999). The computational results of the mass circumferential average loss coefficient profiles along radius height are shown in Fig. 4. It is shown in Fig. 4 (a) that forward sweep reduces losses and backward sweep increases losses in tip region. All sweeps reduces the losses close 50% radial height as shown in Fig.4 (b). Backward sweep has smallest losses in the middle height of the blade. The blade exit loss is the loss sum along whole blade.

The calculated mass average flow angles at the exit section for all the cases show that the flow angles are almost the same. Because the entire sweep study keep the section parameters the same. The flow angles for the backward sweep and baseline cases are shown in Fig. 5. It is shown that the sweep blades keep the same outflow angle as baseline.

The isentropic Mach number at the root section, middle span and tip section are shown in Figs. 6 through 8. You is depicted in the figure, the curve of the Forward Sweep is almost identical to the curve of Part Forward Sweep. Root and tip sections have larger impact than those at the middle sections. For all the sweep cases, the leading edge loadings at the root section are larger than baseline blade. Forward cases reduce the airfoil loading and backward increase the airfoil loading at mid- and tip-sections. These results are similar to those reported by Denton and Xu (1999), but the magnitude of the loading changes is much smaller. In addition, the backward sweep causes the peak suction point close to the leading edge at root section. The reduction in loading at the leading edge could reduce the shock waves. However, if the unsweep blade did not have a strong leading edge shock wave, the impact of the losses due to reduction of the shack strength is not significant. The overall loss then is determined by secondary flow losses. This may be the reason why some researchers (Rabe et al., 1991; Hah et al., 1999) reported the significant losses reductions and others (Wadia et al., 1997) did not.

The axial velocity contours near the suction surface are shown in Fig. 9 (a), where the pick speed region is inclined according to the sweep of the airfoil leading edge. The secondary flow contours for suction and pressure side of the blade are shown in Fig. 9(b) and (c) respectively. It is shown that forward sweep reduce the secondary flow both near tip and root regions. It is also shown that all the sweep cases reduce the secondary flow in middle height of the blade. The secondary flow behind the tip clearance is strongest than other regions. The strong secondary flow in the tip clearance region will increase the entropy generation.

The static pressure distributions near the suction surface are shown in Fig. 10. This figure indicates that the low-pressure region is also inclined according to the leading edge loading. However, the sizes of the low-pressure regions for different sweeps are distinctive. The backward sweep has the largest low-pressure region and the forward sweep has the smallest low-pressure region.

However, the backward sweep does not present much of the losses, perhaps because the inclination of the low-pressure region causes the inclination of the shock, which reduces the losses from shock waves.

The relative Mach number contours between the blades at root, middle and tip sections are shown in Figs. 11 to 13. All the sweep cases have the similar Mach number distributions at root section. However, the location of the peak Mach number near the suction surface moved forward for the backward sweep case, which agrees with the contours of the Isentropic Mach number plotted in Fig. 6. The middle span section Mach number distributions present a different feature after the shock waves. The backward sweep case has a relatively large region for the high Mach number, perhaps because the shock waves are weaker for the backward sweep blade than for other cases. Thus, it causes the shock losses at middle section, and, therefore, it is smaller for the backward sweep case, which again agrees with the losses distributions shown in Fig. 4. The tip section Mach number distributions show that the backward sweep has the strongest shock wave, which causes this section to present high losses.

The total pressure distributions at the exit station are shown in Fig. 14. The results indicate that, for the backward sweep, the high total pressure region at the top section is larger than the other cases. It does not show other obvious differences in the total pressure distributions for all the sweep cases. Because the quantity of the losses for different sweep cases are smaller.

CONCLUSIONS

The effects of the three-dimensional blade sweeps were predicted with a computational fluid dynamics code. The calculations kept all blade design parameters and boundary conditions for all the cases in order to properly present the sweep effects of the airfoil. The calculations showed that the sweep did not cause significant efficiency improvements at current baseline blade. Because the baseline airfoil has a relatively good design as well as shock did not play a important ruler in the overall losses. This study revealed that the forward and backward sweeps had different impact to the secondary flows and shock wave structures. It is important for the turbomachinery designers to understand the baseline loss patterns and then to select the suitable sweep to improve the design.

REFERENCES

Bliss, D.B., 1976, Method of and Apparatus for preventing leading edge shock and shock related noise in Transonic and supersonic blades and like, US Patent 3989406.

Denton, J. D. And Xu, L., 1999, "The exploitation of three-dimensional flow in turbomachinery design," Proc Instn Mech Engrs, Vol 213, part C, pp125-137.

Hah, C, Puterbaugh, S.L. and Wadia, A. R., 1999, "Control of shock structure and secondary flow field inside transonic compressor rotor through aerodynamic sweep," ASME 99-GT-561.

Ho, Y. H. and Lakshminarayana, 1996, "Computational Modeling of Three-Dimensional Endwall Flow Through a Turbine Rotor Cascade with Strong Secondary Flows," J. of Turbomachinery, 118, pp.250-261.

Lakshminarayana, B., 1991, "An Assessment of Computational Fluid Dynamics Techniques in the Analysis and Design of Turbomachinery—The 1990 Freeman Scholar Lecture," ASME J. Fluids Eng., 113, pp.315-352.

Rabe, D., Hoying, D. and Koff, S., 1991, "Application of sweep to improve the efficiency of a transonic fan, part II-performance and laser test results," AIAA paper 91-2544.

Singh, G., Walker, P.J and Haller, B. R., 1995, "Development of 3D stage viscous time marching method for optimisation of short

stage heights", Proc. Of European Conf. On Turbomachinery, Erlangen.

Wadia, A. R., Szucs, P. N. And Crall, W. W., 1997, "Inner workings of aerodynamic sweep," ASME 97-GT-401.

Walker, P.J. and Denton, J. D., 1998, "Comparision of design intent and experimental measurements in a low aspect ratio axial flow turbine with three-dimensional blading," ASME paper 98-GT-516.

Xing, X. Q., Zhou, s. and Zhao, X. L, 2001, "Probing into the connotation of sweep aerodynamics of transonic fans and compressors," ASME 2001-GT-0352.

Xu, C. and Amano, R.S., 2000a, "A Hybrid Numerical Procedure for Cascade Flow Analysis," *Numerical Heat Transfer, Part B*, Vol. 37, No. 2, pp. 141-164.

Xu, C. and Amano, R. S., 2000b, "An Implicit Scheme for Cascade Flow and Heat Transfer Analysis," ASME J. of Turbomachinery, Vol. 122, pp. 294-300.

Xu, C. and Amano R.S., 2001a "On the Development of Turbine Blade Aerodynamic Design System," ASME IGTI Turbo & Expo, 2001-GT-0443.

Xu, C. and Amano R.S., 2001b, "Computational Analysis of Pitch Width Effects on the Losses of Turbine Blades," 2001 ASME DETC CIE, Pittsburgh, PA.

Xu and R. S. Amano, "Turbomachinery Blade Aerodynamic Design and Optimization," GT-2002-30541, 2002.

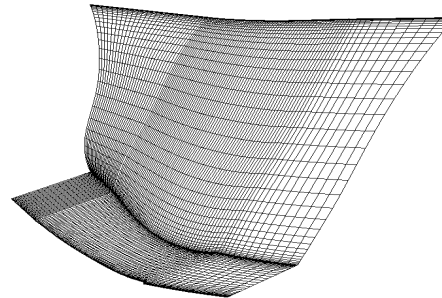


Figure1. Mesh distribution.

Table 1. Total loss coefficient.

Sweep type	Baseline	Forward	Backward	Part
Total loss co. (%)	2.87	2.81	2.89	2.85

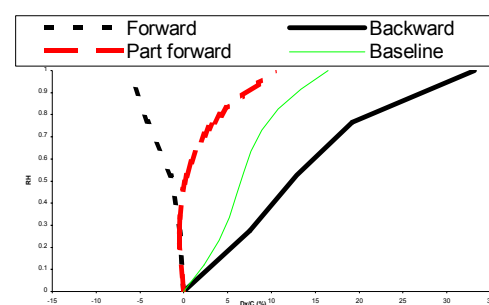


Figure 2. Sweep definition.

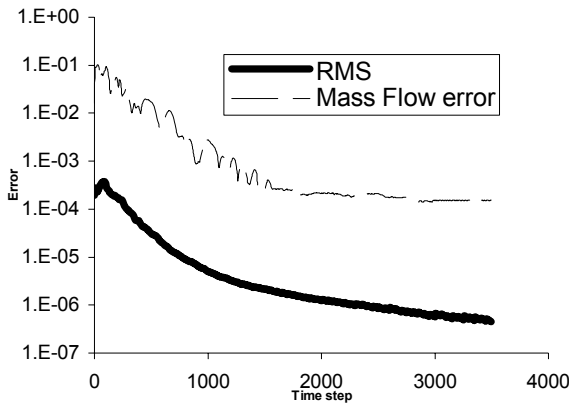
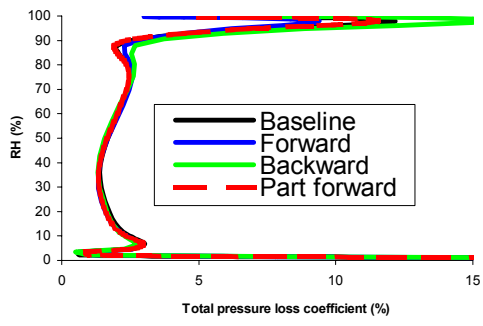
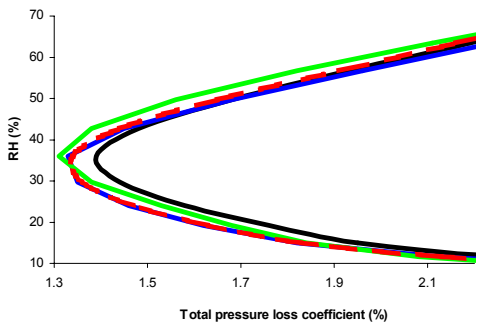


Figure 3. Convergence history.



(a). Total pressure loss coefficient distribution for whole spanwise



(b). Total pressure loss coefficient distribution near middle span

Figure 4. Total pressure loss coefficient distributions.

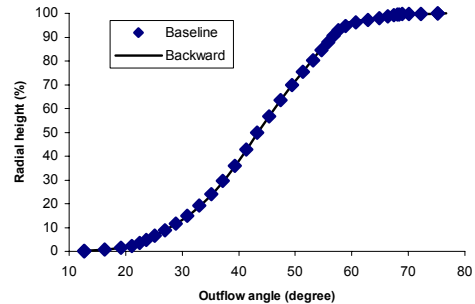


Figure 5. Mass average outflow angles.

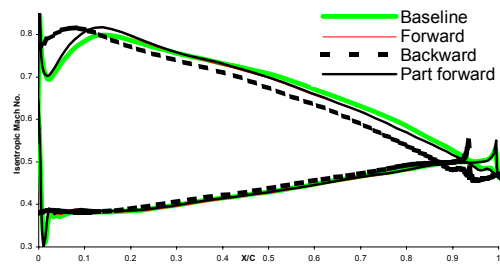


Figure 6. Isentropic Mach Number distribution at root section.

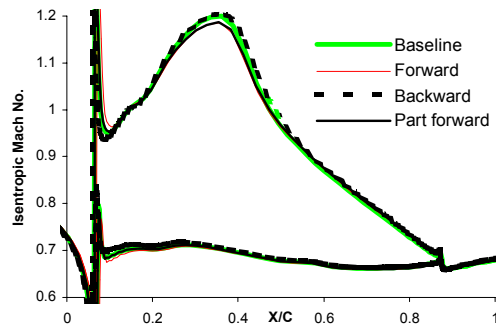


Figure 7. Isentropic Mach Number distribution at middle span.

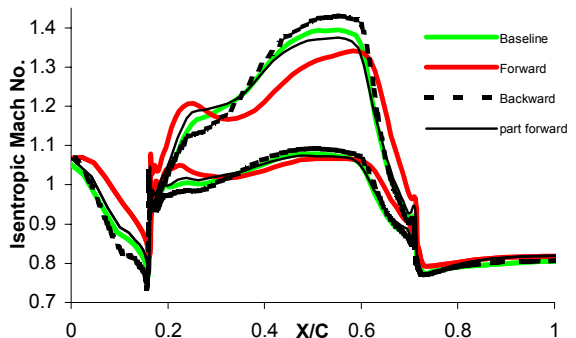


Figure 8. Isentropic Mach Number distribution at tip section.

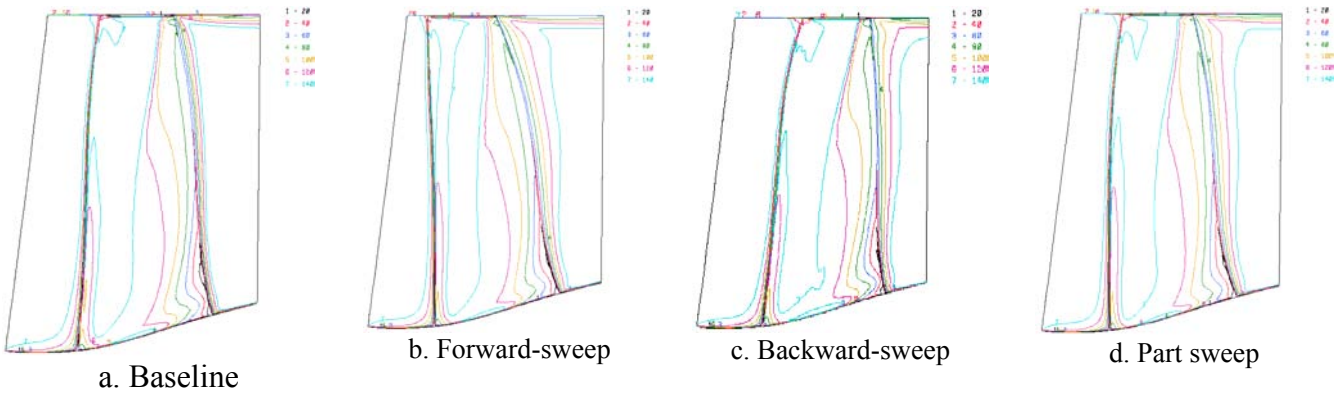


Figure 9(a). Axial velocity contour near the suction side.

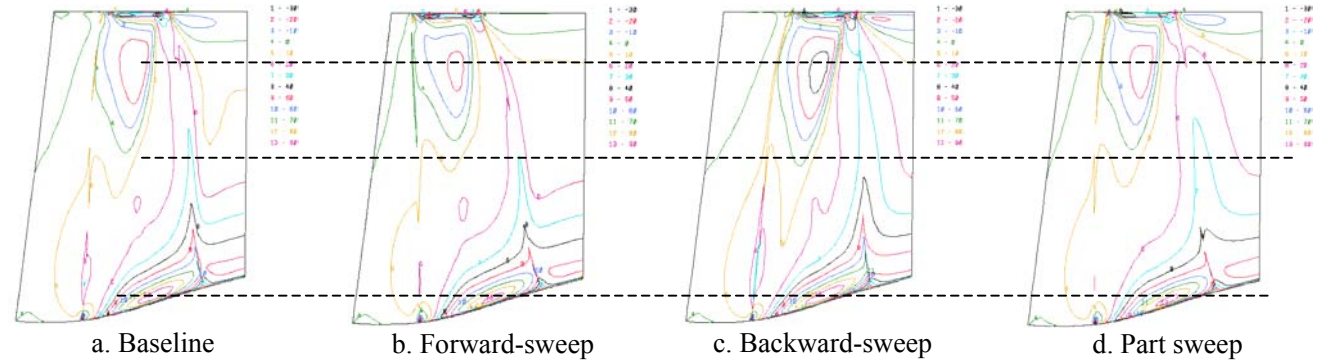


Figure 9(b). Radial secondary flow contour near the suction side.

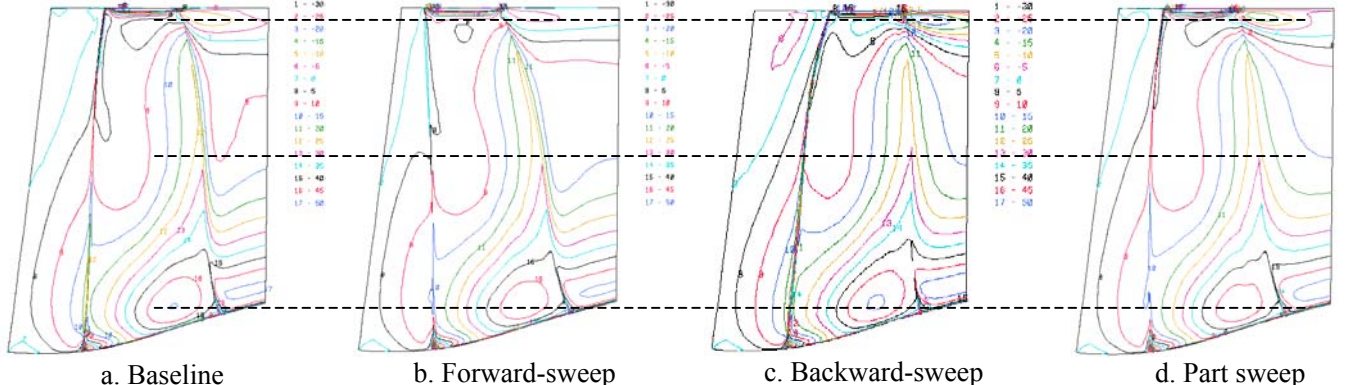


Figure 9(c). Radial secondary flow contour near the pressure side.

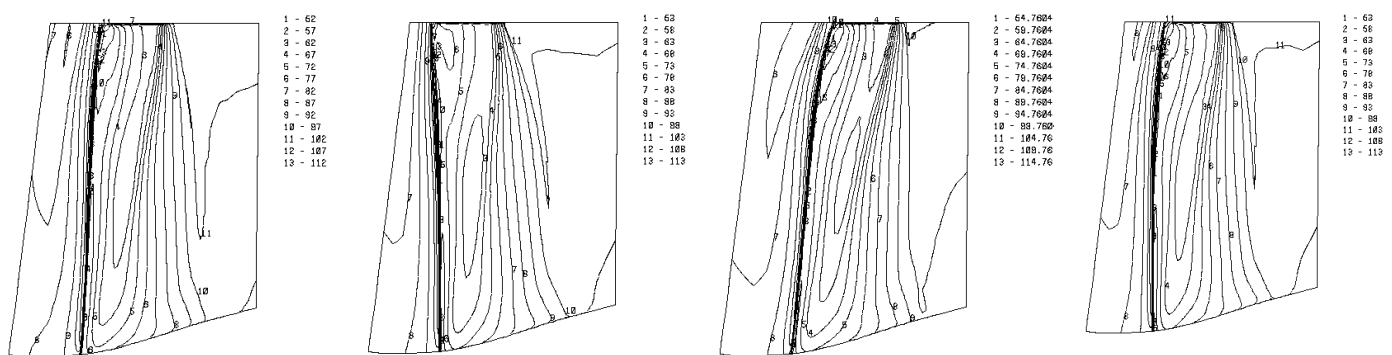


Figure 10. Static pressure near the suction side.

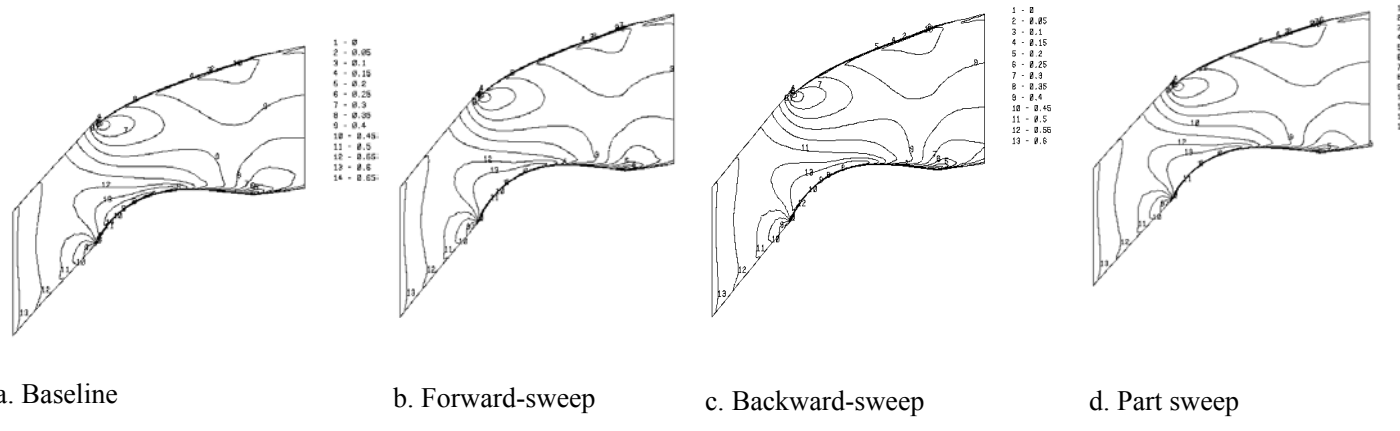


Figure 11. Relative Mach number contour near root section.

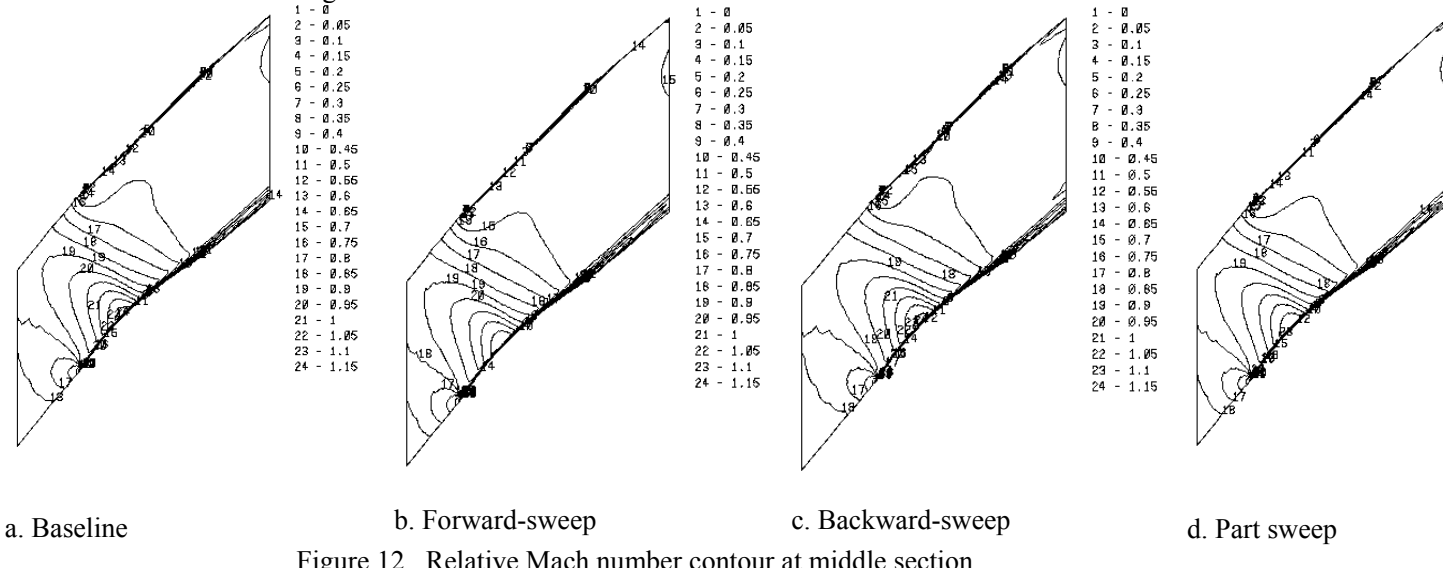


Figure 12. Relative Mach number contour at middle section.

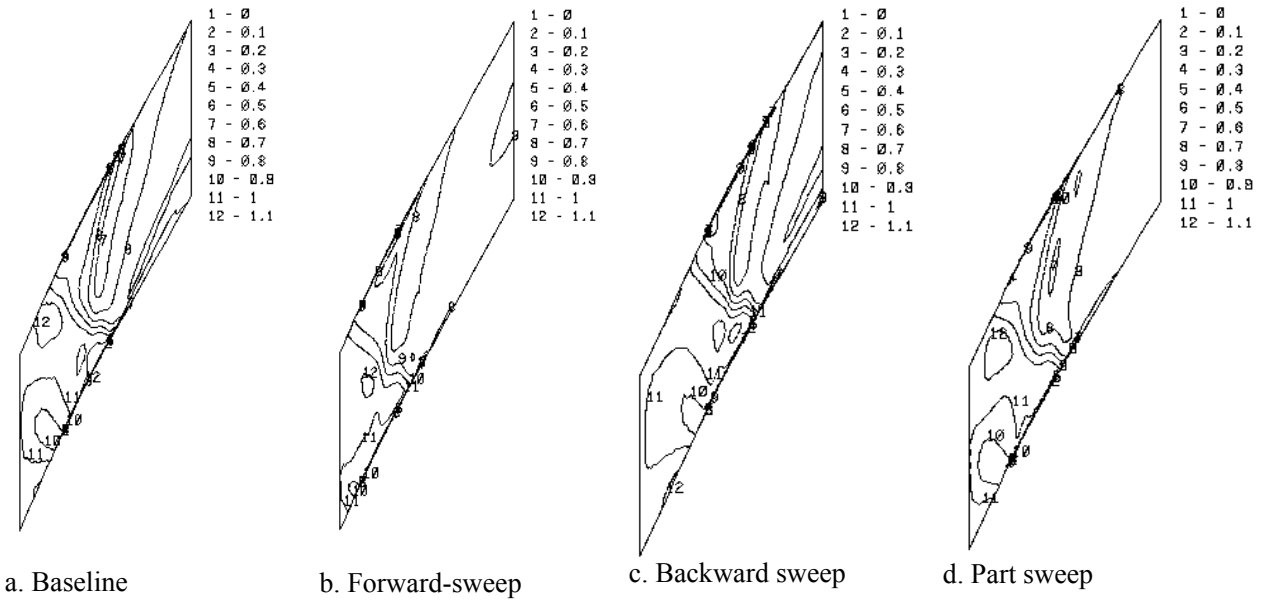


Figure 13. Relative Mach number contour near tip section.

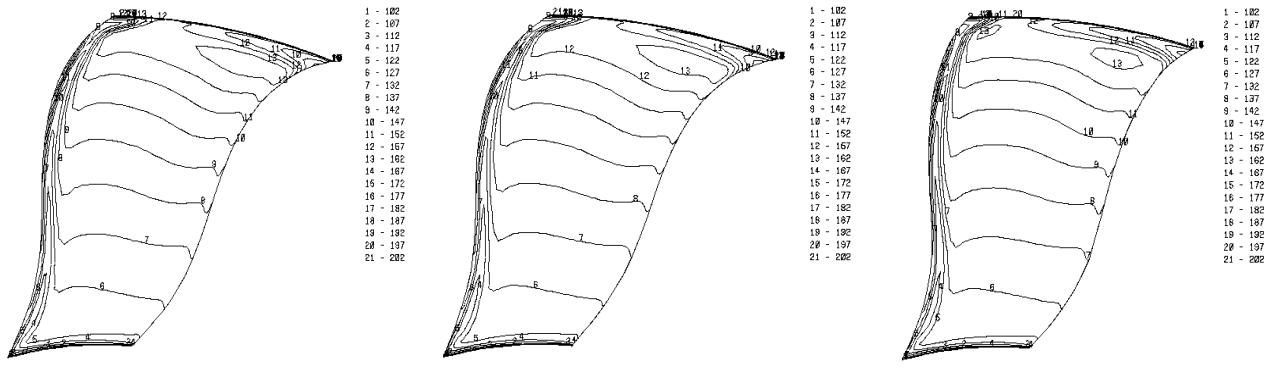


Figure 14. Total pressure distributions at exit plan.